

Two-band model of Raman scattering on electron-doped high- T_c superconductor

C. S. Liu,^{1,2} H. G. Luo,¹ W. C. Wu,² and T. Xiang^{1,3}

¹*Institute of Theoretical Physics and Interdisciplinary Center of Theoretical Studies,
Chinese Academy of Sciences, P. O. Box 2735, Beijing 100080, China*

²*Department of Physics, National Taiwan Normal University, Taipei 11650, Taiwan*

³*Center for Advanced Study, Tsinghua University, Beijing 100084, China*

We have analyzed the B_{1g} and B_{2g} Raman spectra of electron-doped cuprate superconductors $\text{Nd}_{2-x}\text{Ce}_x\text{CuO}_4$ and $\text{Pr}_{2-x}\text{Ce}_x\text{CuO}_4$ using a weakly coupled two-band model. One of these two bands is centered around $(\pm\pi/2, \pm\pi/2)$ and couples more strongly with the B_{2g} mode, while the other is centered around $(\pm\pi, 0)$ and $(0, \pm\pi)$ and couples more strongly with the B_{1g} mode. This model explains in a natural way why the B_{2g} Raman peak occurs at a higher frequency than the B_{1g} one at optimal doping, and how these two peaks change with doping in agreement with experiments. The result thus supports that there are two kinds of quasiparticles in electron-doped cuprates and $d_{x^2-y^2}$ -wave superconductivity is driven by the holelike band and a proximity effect on the electronlike band.

PACS numbers: 74.25.Gz, 74.20.Mn, 74.20.Rp 78.30.-j

I. INTRODUCTION

Pairing symmetry of electron-doped high- T_c cuprate superconductors such as $\text{Nd}_{2-x}\text{Ce}_x\text{CuO}_4$ and $\text{Pr}_{2-x}\text{Ce}_x\text{CuO}_4$ is a long standing problem [1, 2, 3, 4, 5, 6, 7, 8, 9, 10, 11, 12, 13, 14, 15, 16, 17]. Although no consensus has been reached yet, more and more recent experimental results have suggested that the order parameter of electron-doped cuprates is likely to have $d_{x^2-y^2}$ -wave pairing symmetry [1, 2, 3, 5, 9, 10, 14, 16, 17], in close resemblance to that of hole-doped materials. Among various experiments, the Raman scattering seems to suggest a different story [13, 14, 15]. For hole-doped superconductors, it was known that typical B_{1g} , B_{2g} , and A_{1g} pair-breaking peaks appear, respectively, at the frequencies of 2, 1.6, and 1.2 times of the gap amplitude [18]. However, in electron-doped materials the relative position of the B_{1g} and B_{2g} peaks changes with doping. The B_{2g} peak appears first at a higher frequency than the B_{1g} one in the underdoped regime. It then moves down and finally appears at a frequency lower than that of the B_{1g} peak in the heavily overdoped regime.

The Raman scattering has the potential to probe different regions of the Fermi surface (FS), thus a thorough understanding of the experimental data can provide a better understanding on the momentum dependence of superconducting (SC) pairing gap. The observation of B_{2g} Raman peak at higher frequency than that of B_{1g} would imply a non-monotonic $d_{x^2-y^2}$ -wave order parameter in a single-band system [14]. This nonmonotonic order parameter seems to be also consistent with the observation of angle resolved photoemission spectroscopy (ARPES) [16]. However, this one-band picture may not be adequate to describe the nature of two kinds of charge carriers in electron-doped cuprate superconductors, as revealed by magneto-transport measurements [19, 20, 21].

A key clue towards the understanding of Raman data in $\text{Nd}_{2-x}\text{Ce}_x\text{CuO}_4$ comes from the doping evolution of

the FS revealed by ARPES [22, 23]. At low doping, four small FS pockets first appear around $(\pm\pi, 0)$ and $(0, \pm\pi)$. By increasing the doping, four new pockets begin to form around $(\pm\pi/2, \pm\pi/2)$. These results can be explained in terms of the \mathbf{k} -dependent band-folding effect due to antiferromagnetic (AF) ordering. The original band is folded back into the magnetic Brillouin zone (MBZ) around the diagonal line $(\pi, 0) \rightarrow (0, \pi)$. Near the intersecting points of the Fermi surface, an AF gap opens and splits the original FS into two [24, 25, 26]. This two-band picture was first used by Luo and Xiang to explain the unusual temperature dependence of the magnetic penetration depth in electron-doped copper oxides [27]. It is supported by Hall coefficient and magneto-resistance measurements [19, 20, 21]. The generic feature of a weakly coupled two-band model was discussed in Ref. [28] in the context of hole-doped cuprate superconductors.

In this paper, we shall use a two-band model to study the Raman response for the electron-doped cuprates. As will be shown, the two-band model gives a unified explanation to the unusual behaviors of Raman spectra. It explains in a natural way why the B_{2g} Raman peak appears at a higher frequency than that of the B_{1g} peak at optimal doping and why the relative positions of these two peaks change in the heavily overdoped regime.

II. MODEL AND FORMALISM

We start by considering the two-dimensional t - t' - t'' - J model

$$H = -t \sum_{\langle ij \rangle_{1\sigma}} c_{i\sigma}^\dagger c_{j\sigma} - t' \sum_{\langle ij \rangle_{2\sigma}} c_{i\sigma}^\dagger c_{j\sigma} - t'' \sum_{\langle ij \rangle_{3\sigma}} c_{i\sigma}^\dagger c_{j\sigma} + J \sum_{\langle ij \rangle} \left(\vec{S}_i \cdot \vec{S}_j - \frac{1}{4} n_i n_j \right), \quad (1)$$

where $\langle ij \rangle_1$, $\langle ij \rangle_2$, and $\langle ij \rangle_3$ denote the nearest, second-nearest, and third-nearest neighbors between i and j . No

double occupied sites are allowed in Eq. (1). All notations used in (1) are standard. Applying the slave-boson and MF decoupling [25], Hamiltonian (1) can be written in terms of two (diagonalized) bands in momentum space

$$H = \sum'_{\mathbf{k}\sigma} (\xi_{\mathbf{k}\alpha} \alpha_{\mathbf{k}\sigma}^\dagger \alpha_{\mathbf{k}\sigma} + \xi_{\mathbf{k}\beta} \beta_{\mathbf{k}\sigma}^\dagger \beta_{\mathbf{k}\sigma}),$$

where the prime denotes that the momentum summation is over the MBZ only ($-\pi < k_x \pm k_y \leq \pi$) and

$$\xi_{\mathbf{k},l} = \frac{\varepsilon_{\mathbf{k}} + \varepsilon_{\mathbf{k}+\mathbf{Q}}}{2} \mp \sqrt{\frac{(\varepsilon_{\mathbf{k}+\mathbf{Q}} - \varepsilon_{\mathbf{k}})^2}{4} + 4J^2 m^2}$$

with $\mathbf{Q} \equiv (\pi, \pi)$ the AF wave vector and $m \equiv (-1)^i \langle S_i^z \rangle$ the AF order. Here

$$\begin{aligned} \varepsilon_{\mathbf{k}} &= (2|t|\delta - J\chi) (\cos k_x + \cos k_y) \\ &- 4t'\delta \cos k_x \cos k_y - 2t''\delta (\cos 2k_x + \cos 2k_y) \end{aligned} \quad (2)$$

with $\chi \equiv \langle f_{i\sigma}^\dagger f_{j\sigma} \rangle$ the uniform bond order and δ the doping concentration ($f_{i\sigma}$ is the fermionic spinon operator).

In the SC state, we add a BCS coupling term to each band and assume the system to be described by the following Hamiltonian [27]

$$H = \sum'_{\mathbf{k}\sigma l} \xi_{\mathbf{k}l} l_{\mathbf{k}\sigma}^\dagger l_{\mathbf{k}\sigma} + \sum'_{\mathbf{k}l} \Delta_{\mathbf{k}l} (l_{\mathbf{k}\uparrow}^\dagger l_{-\mathbf{k}\downarrow}^\dagger + l_{-\mathbf{k}\downarrow} l_{\mathbf{k}\uparrow}),$$

where $l \equiv \alpha, \beta$ and $\Delta_{\mathbf{k},l} = (\Delta_l/2) [\cos k_x - \cos k_y]$ are the $d_{x^2-y^2}$ -wave gap functions.

The Raman scattering intensity is proportional to the imaginary part of the effective density-density correlation function $\chi(\mathbf{q}, \tau) = \langle T_\tau [\tilde{\rho}(\mathbf{q}, \tau), \tilde{\rho}(-\mathbf{q}, 0)] \rangle$ in the limit $\mathbf{q} \rightarrow 0$. Here $\tilde{\rho}(\mathbf{q}, \tau) \equiv \sum_{\mathbf{k}, \sigma} \gamma_{\mathbf{k}} \sigma c_{\mathbf{k}+\mathbf{q}}^\dagger(\tau) c_{\mathbf{k}}(\tau)$ is the effective density operator and $\gamma_{\mathbf{k}}$ is the Raman vertex. When the energy of incident light is smaller than the optical band gap, the contribution from the resonance channel is negligible. The Raman vertex can then be obtained in terms of the curvature of the band dispersion under the inverse effective mass approximation.

In the current two-band model, the effective density operator is decomposed as

$$\begin{aligned} \tilde{\rho}(\mathbf{q}, \tau) &\equiv \sum'_{\mathbf{k}, \sigma} [\gamma_{\mathbf{k}} c_{\mathbf{k}+\mathbf{q}, \sigma}^\dagger(\tau) c_{\mathbf{k}, \sigma}(\tau) \\ &+ \gamma_{\mathbf{k}+\mathbf{Q}} c_{\mathbf{k}+\mathbf{Q}+\mathbf{q}, \sigma}^\dagger(\tau) c_{\mathbf{k}+\mathbf{Q}, \sigma}(\tau)]. \end{aligned} \quad (3)$$

Along with the unitary transformation [25] such that operators $c_{\mathbf{k}}$ and $c_{\mathbf{k}+\mathbf{Q}}$ are transformed into $\alpha_{\mathbf{k}}$ and $\beta_{\mathbf{k}+\mathbf{Q}}$, the Raman response function for each symmetric channel (S) is then given by [29]

$$\begin{aligned} \chi^S(\mathbf{q} \rightarrow 0, \tau) &= - \sum'_{\mathbf{k}, ll'} (\gamma_{\mathbf{k}, ll'}^S)^2 [\mathcal{G}_l(\mathbf{k}, \tau) \mathcal{G}_{l'}(\mathbf{k}, -\tau) \\ &- \epsilon_{ll'} \mathcal{F}_l(\mathbf{k}, \tau) \mathcal{F}_{l'}(\mathbf{k}, -\tau)], \end{aligned} \quad (4)$$

where \mathcal{G} and \mathcal{F} are the normal and anomalous Green functions for a superconductor, $\epsilon_{ll'} = 1$ if $l = l'$ or -1 if $l \neq l'$. The intra- and interband vertex functions are

$$\begin{aligned} \gamma_{\mathbf{k}, \alpha\alpha}^S &= \cos^2 \theta_{\mathbf{k}} \gamma_{\mathbf{k}}^S + \sin^2 \theta_{\mathbf{k}} \gamma_{\mathbf{k}+\mathbf{Q}}^S, \\ \gamma_{\mathbf{k}, \beta\beta}^S &= \sin^2 \theta_{\mathbf{k}} \gamma_{\mathbf{k}}^S + \cos^2 \theta_{\mathbf{k}} \gamma_{\mathbf{k}+\mathbf{Q}}^S, \\ \gamma_{\mathbf{k}, \alpha\beta}^S &= \gamma_{\mathbf{k}, \beta\alpha}^S = \sin 2\theta_{\mathbf{k}} (\gamma_{\mathbf{k}}^S - \gamma_{\mathbf{k}+\mathbf{Q}}^S), \end{aligned} \quad (5)$$

where $\cos 2\theta_{\mathbf{k}} \equiv (\varepsilon_{\mathbf{k}+\mathbf{Q}} - \varepsilon_{\mathbf{k}}) / \sqrt{(\varepsilon_{\mathbf{k}+\mathbf{Q}} - \varepsilon_{\mathbf{k}})^2 + 4J^2 m^2}$. For the B_{1g} and B_{2g} channels, $\gamma_{\mathbf{k}}^{B_{1g}} = \gamma_{\mathbf{k}}^{xx} - \gamma_{\mathbf{k}}^{yy}$ and $\gamma_{\mathbf{k}}^{B_{2g}} = 2\gamma_{\mathbf{k}}^{xy}$. Here $\gamma_{\mathbf{k}}^{ij} \equiv \partial^2 \varepsilon_{\mathbf{k}} / \partial k_i \partial k_j$ (inverse effective mass approximation). Eq. (4) and (5) reduce to the famous ones in a one-band system when $m = 0$ [18].

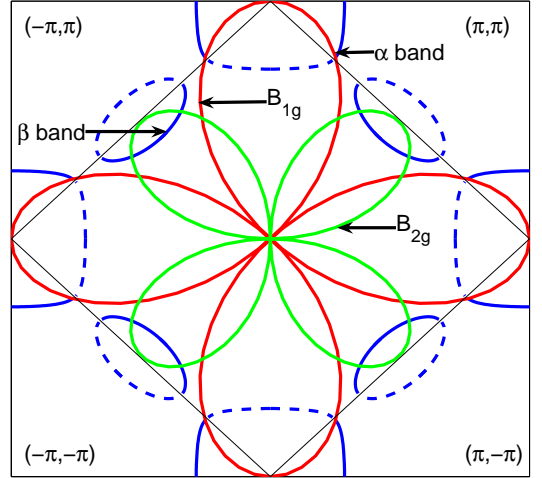


FIG. 1: Schematic plot of the Fermi surfaces for the α and β bands and the momentum dependence of the B_{1g} and B_{2g} Raman vertices. The B_{1g} and B_{2g} modes couple more strongly with the α and β bands, respectively.

Shown in Fig. 1 are the B_{2g} and B_{1g} Raman vertices and how they are coupled to the SC quasiparticle excitations in \mathbf{k} space. Since the B_{2g} vertex has d_{xy} symmetry, the B_{2g} channel is dominated by the excitations of the β band. In contrast, the B_{1g} vertex has $d_{x^2-y^2}$ symmetry, thus the B_{1g} channel is contributed mainly from the excitations of the α band. Since both B_{2g} and B_{1g} vertices are odd-parity, their Raman intensities are not affected by the Coulomb screening. For the fully symmetric A_{1g} channel, in contrast, all regions of momentum space contribute and the Raman intensity is partially screened. Since the A_{1g} channel is more sensitive to the actual vertex as well as the screening effect, we will leave out A_{1g} and focus on the B_{2g} and B_{1g} channels only.

In electron doped cuprates, the SC state appears only when the β band emerges above the Fermi energy. This would suggest that we assume that it is the β band that drives the system to superconduct, while the α band becomes superconducting mainly via the proximity effect. A simple picture for the understanding of the unusual Raman spectra in electron doped cuprates can then be

sketched as follows. In the under doped or optimally doped regime, the β band couples more strongly with the AF fluctuations than the α band. This results in a relatively larger SC gap in the β band (Δ_β) than in the α band (Δ_α). The B_{1g} channel probes mainly the quasi-particle (QP) excitations of the α band, thus the B_{1g} Raman peak is mainly determined by Δ_α . Similarly, the B_{2g} channel probes mainly the QP excitations of the β band, its Raman peak is mainly determined by Δ_β . If Δ_α is much smaller than Δ_β , one would then expect that the B_{1g} peak appears at a frequency lower than that of the B_{2g} peak, unlike in the hole doped case. In the heavily overdoped regime, the AF correlation becomes very weak and the band splitting vanishes. In this case the two-band model reduces essentially to a one-band model and the B_{1g} and B_{2g} Raman spectra would behave similarly as in the hole doped cuprate superconductors, consistent with the experiments.

III. RESULTS AND DISCUSSIONS

A. On $\text{Nd}_{2-x}\text{Ce}_x\text{CuO}_4$

Pertaining to $\text{Nd}_{2-x}\text{Ce}_x\text{CuO}_4$, we have adopted $|t| = 0.326$ eV, $t' = 0.3t$, $t'' = -0.2t$, and $J = 0.3t$ to simulate the band structure [25]. We take $\chi = -0.15$ and $m = 0.178$ for the optimally doped ($x = 0.15$) sample, $\chi = -0.15$ and $m = 0.15$ for the overdoped ($x = 0.16$) sample. These parameters are close to those obtained in self-consistent calculations for the normal states [25]. The chemical potentials are determined by the filling factor for each band to give the true doping concentration through $x = n_e - n_h$.

Theoretical fitting procedures are implemented as follows. First, the vertex functions are evaluated using (5). Then the SC gaps Δ_α and Δ_β and the smearing Lorentz width Γ_α and Γ_β are adjusted to fit the peak positions and the overall spectral line shape (up to a constant multiplying factor).

Figure 2 compares the experimental data of Raman spectra for $\text{Nd}_{2-x}\text{Ce}_x\text{CuO}_4$ with the theoretical calculations. For all the cases considered in Fig. 2, our fitting curves are in good agreement with the experimental results. For the optimally doped sample ($x=0.15$) reported in Ref. [14] at $T = 8$ K (first column), the B_{1g} and B_{2g} Raman peaks appear at 50 cm^{-1} and 55 cm^{-1} , respectively. The corresponding gap and smearing parameters obtained by fitting are $(\Delta_\alpha, \Delta_\beta) = (21$ $\text{cm}^{-1}, 48$ $\text{cm}^{-1})$ and $(\Gamma_\alpha, \Gamma_\beta) = (6$ $\text{cm}^{-1}, 8$ $\text{cm}^{-1})$. The ratio between the B_{1g} Raman peak frequency and Δ_α is about 2.4, while the ratio between the B_{2g} Raman peak frequency and Δ_β is about 1.2. The corresponding ratios in a hole doped $d_{x^2-y^2}$ -wave superconductor are about 2 and 1.6, respectively. This difference between hole and electron doped cuprates is not difficult to be understood. In electron doped materials, the AF correlation splits the continuous FS into two separate sheets. This then suppresses the

TABLE I: Summary of fitting parameters for $\text{Nd}_{2-x}\text{Ce}_x\text{CuO}_4$ (refer to Fig. 2).

	Column 1	Column 2	Column 3
T_c (K)	22	22	13
m	0.178	0.178	0.15
Γ_α (cm^{-1})	6	4	8
Γ_β (cm^{-1})	8	6	8
Δ_α (cm^{-1})	21	27	21
Δ_β (cm^{-1})	48	57	37
$\Delta_\beta/\Delta_\alpha$	2.29	2.11	1.76
Δ_β/T_c	2.18	2.59	2.84

high (low) energy region to which the B_{2g} (B_{1g}) probes. It is thus expected that the B_{2g} (B_{1g}) peak will be red shifted (blue shifted) compared with the result of hole-doped cuprate superconductors.

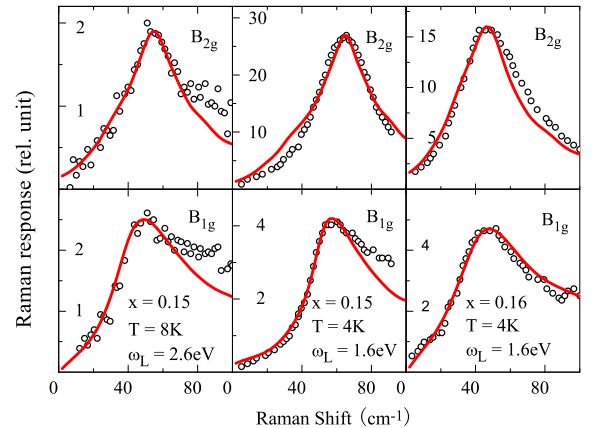


FIG. 2: Comparison of the theoretical calculations (solid lines) with the measurement data (circles) for $\text{Nd}_{2-x}\text{Ce}_x\text{CuO}_4$. The experimental data in the first column are taken from Ref. [14]. The data in the second and third columns are taken from Ref. [15]. ω_L is the incident photon energy.

For another set of data of the optimally doped sample reported in Ref. [15] at $T = 4$ K (second column), the fitting parameters are $(\Delta_\alpha, \Delta_\beta) = (27$ $\text{cm}^{-1}, 57$ $\text{cm}^{-1})$ and $(\Gamma_\alpha, \Gamma_\beta) = (4$ $\text{cm}^{-1}, 6$ $\text{cm}^{-1})$. The corresponding parameters for the overdoped sample at $T = 4$ K (third column) are $(\Delta_\alpha, \Delta_\beta) = (21$ $\text{cm}^{-1}, 37$ $\text{cm}^{-1})$ and $\Gamma_\alpha = \Gamma_\beta = 8$ cm^{-1} . The gap parameters obtained are consistent with the general expectation. Both Δ_α and Δ_β decrease with increasing temperature at the same doping level and with increasing doping at the same temperature. The gap ratio, $r \equiv \Delta_\beta/\Delta_\alpha$, is reduced from 2 at optimal doping to 1.7 at slightly overdoping, consistent with the scenario of AF-like fluctuation induced superconductivity. All fitting parameters for $\text{Nd}_{2-x}\text{Ce}_x\text{CuO}_4$ are summarized in Table I.

TABLE II: Summary of fitting parameters for $\text{Pr}_{2-x}\text{Ce}_x\text{CuO}_4$ (refer to Fig. 3).

	Column 1	Column 2	Column 3
x	0.15	0.165	0.18
T_c (K)	23.5	15	10
m	0.15	0.12	0
$\Gamma_\alpha(\text{cm}^{-1})$	6	8	15
$\Gamma_\beta(\text{cm}^{-1})$	6	8	15
$\Delta_\alpha(\text{cm}^{-1})$	31	16	15
$\Delta_\beta(\text{cm}^{-1})$	68	30	15
$\Delta_\beta/\Delta_\alpha$	2.19	1.88	1
Δ_β/T_c	2.89	2	1.5

B. On $\text{Pr}_{2-x}\text{Ce}_x\text{CuO}_4$

The Raman scattering measurement has also been carried out in electron-doped $\text{Pr}_{2-x}\text{Ce}_x\text{CuO}_4$ at various doping levels [15]. The Raman spectra of $\text{Pr}_{2-x}\text{Ce}_x\text{CuO}_4$, as shown in Fig. 3, behave similarly as for $\text{Nd}_{2-x}\text{Ce}_x\text{CuO}_4$. At optimal doping, the B_{2g} peak appears at a frequency higher than that of the B_{1g} peak. With increasing doping, the frequency of the B_{1g} peak approaches to and finally surpasses the B_{2g} peak in the overdoped regime.

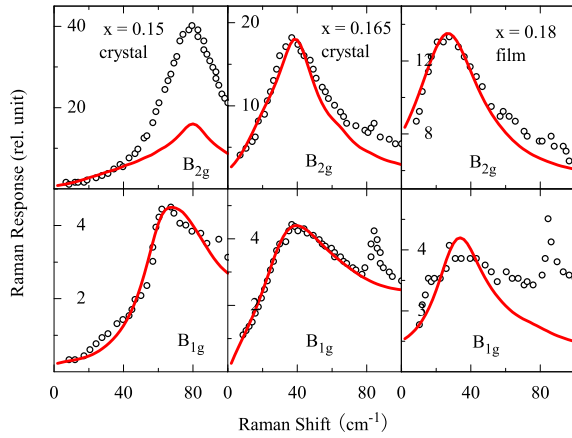


FIG. 3: Comparison between the theoretical results (solid curves) and the Raman measurement data from Ref. [15] (circles) for $\text{Pr}_{2-x}\text{Ce}_x\text{CuO}_4$ at $T = 4\text{K}$. $\omega_L = 1.9\text{eV}$.

Figure. 3 compares the measurement data of $\text{Pr}_{2-x}\text{Ce}_x\text{CuO}_4$ with our theoretical calculations. For the optimally doped sample ($x = 0.15$), the Raman peak appears at 80 cm^{-1} for the B_{2g} mode and at 62 cm^{-1} for the B_{1g} mode. The parameters obtained by fitting are $(\Delta_\alpha, \Delta_\beta) = (31\text{ cm}^{-1}, 68\text{ cm}^{-1})$ and $\Gamma_\alpha = \Gamma_\beta = 6\text{ cm}^{-1}$, with $\chi = -0.15$ and $m = 0.15$. For the slightly overdoped sample ($x = 0.165$), the B_{2g} and B_{1g} peaks ap-

pear at the same frequency at 37 cm^{-1} and the parameters we obtained are $(\Delta_\alpha, \Delta_\beta) = (16\text{ cm}^{-1}, 30\text{ cm}^{-1})$ and $\Gamma_\alpha = \Gamma_\beta = 8\text{ cm}^{-1}$, with $\chi = -0.15$ and $m = 0.12$. For the heavily over-doped sample ($x = 0.18$), the Raman peaks appear at 25 cm^{-1} and 30 cm^{-1} for the B_{2g} and B_{1g} modes, respectively. The relative peak positions of these two modes are similar as in a one-band $d_{x^2-y^2}$ -wave superconductor. This is not unexpected since at such a high doping level, the two-band model reduces essentially to a one-band model. In this case, the parameters we obtained are $\Delta_\alpha = \Delta_\beta = 15\text{ cm}^{-1}$ and $\Gamma_\alpha = \Gamma_\beta = 15\text{ cm}^{-1}$, with $\chi = -0.15$ and $m = 0$. For the above three samples, the ratio $\Delta_\beta/\Delta_\alpha$ changes from 2.3, to 1.9, and finally to 1 with increasing doping. With increasing doping, the AF order is depressed and the gap amplitudes is decreased. The results are consistent with neutron scattering measurement [30]. All fitting parameters for $\text{Pr}_{2-x}\text{Ce}_x\text{CuO}_4$ are summarized in TABLE II.

In the top-left panel of Fig. 3 for the B_{2g} mode, the experimental data are taken under the strong *resonant* regime as emphasized in Refs. [14, 15]. In this case, the contribution from the resonance channel becomes important and the inverse effective mass approximation is not valid. Our theoretical result including only the non-resonant contribution can give a good explanation to the low-frequency part of the spectrum, but the height of the peak is much lower than the experimental one. The resonance channel may also have some contribution to the B_{2g} spectrum in the second column of Fig. 2 for $\text{Nd}_{2-x}\text{Ce}_x\text{CuO}_4$.

IV. SUMMARY

In summary, we have analyzed the Raman spectra of electron-doped cuprate superconductors based on a weakly coupled two-band model. Our result gives a unified explanation to the experimental data in the whole doping range. It suggests strongly that the SC pairing in electron-doped cuprate superconductors results from the same pairing mechanism as in hole doped ones and the gap parameter has $d_{x^2-y^2}$ -wave symmetry. To understand the Raman data in the strong resonance regime, a more comprehensive theory including the contribution from the resonance channel is desired.

Acknowledgments

The authors are grateful to Hsiang-Lin Liu for useful comments on Raman experiments. This work was supported by the National Natural Science Foundation of China (Grant No. 10347149), National Basic Research Program of China (Grant No. 2005CB32170X), and National Science Council of Taiwan (Grant No. 93-2112-M-003-015).

-
- [1] C. C. Tsuei and J. R. Kirtley, Phys. Rev. Lett. **85**, 182 (2000).
- [2] N. P. Armitage, D. H. Lu, D. L. Feng, C. Kim, A. Damascelli, K. M. Shen, F. Ronning, Z.-X. Shen, Y. Onose, Y. Taguchi, et al., Phys. Rev. Lett. **86**, 1126 (2001).
- [3] T. Sato, T. Kamiyama, T. Takahashi, K. Kurahashi, and K. Yamada, Science **291**, 1517 (2001).
- [4] L. Alff, S. Meyer, S. Kleefisch, U. Schoop, A. Marx, H. Sato, M. Naito, and R. Gross, Phys. Rev. Lett. **83**, 2644 (1999).
- [5] R. Prozorov, R. W. Giannetta, P. Fournier, and R. L. Greene, Phys. Rev. Lett. **85**, 3700 (2000).
- [6] J. A. Skinta, M.-S. Kim, T. R. Lemberger, T. Greibe, and M. Naito, Phys. Rev. Lett. **88**, 207005 (2002).
- [7] M.-S. Kim, J. A. Skinta, T. R. Lemberger, A. Tsukada, and M. Naito, Phys. Rev. Lett. **91**, 087001 (2003).
- [8] A. Biswas, P. Fournier, M. M. Qazilbash, V. N. Smolyaninova, H. Balci, and R. L. Greene, Phys. Rev. Lett. **88**, 207004 (2002).
- [9] B. Chesca, K. Ehrhardt, M. Mössle, R. Straub, D. Koelle, R. Kleiner, and A. Tsukada, Phys. Rev. Lett. **90**, 057004 (2003).
- [10] B. Chesca, M. Seifried, T. Dahm, N. Schopohl, D. Koelle, R. Kleiner, and A. Tsukada, Phys. Rev. B **71**, 104504 (2005).
- [11] L. Shan, Y. Huang, H. Gao, Y. Wang, S. L. Li, P. C. Dai, F. Zhou, J. W. Xiong, W. X. Ti, and H. H. Wen, Phys. Rev. B **72**, 144506 (2005).
- [12] H. Balci and R. L. Greene, Phys. Rev. Lett. **93**, 067001 (2004).
- [13] B. Stadlober, G. Krug, R. Nemetschek, R. Hackl, J. L. Cobb, and J. T. Markert, Phys. Rev. Lett. **74**, 4911 (1995).
- [14] G. Blumberg, A. Koitzsch, A. Gozar, B. S. Dennis, C. A. Kendziora, P. Fournier, and R. L. Greene, Phys. Rev. Lett. **88**, 107002 (2002).
- [15] M. M. Qazilbash, B. S. Dennis, C. A. Kendziora, H. Balci, R. L. Greene, and G. Blumberg, cond-mat/0501362; M. M. Qazilbash, A. Koitzsch, B. S. Dennis, A. Gozar, H. Balci, C. A. Kendziora, R. L. Greene, and G. Blumberg, cond-mat/0510098.
- [16] H. Matsui, K. Terashima, T. Sato, T. Takahashi, M. Fujita, and K. Yamada, Phys. Rev. Lett. **95**, 017003 (2005).
- [17] Ariando, D. Darminto, H. J. H. Smilde, V. Leca, D. H. A. Blank, H. Rogalla, and H. Hilgenkamp, Phys. Rev. Lett. **94**, 167001 (2005).
- [18] T. P. Devereaux and D. Einzel, Phys. Rev. B **51**, 16336 (1995).
- [19] Z. Z. Wang, T. R. Chien, N. P. Ong, J. M. Tarascon, and E. Wang, Phys. Rev. B **43**, 3020 (1991).
- [20] W. Jiang, S. N. Mao, X. X. Xi, X. Jiang, J. L. Peng, T. Venkatesan, C. J. Lobb, and R. L. Greene, Phys. Rev. Lett. **73**, 1291 (1994).
- [21] P. Fournier, X. Jiang, W. Jiang, S. N. Mao, T. Venkatesan, C. J. Lobb, and R. L. Greene, Phys. Rev. B **56**, 14149 (1997).
- [22] N. P. Armitage, F. Ronning, D. H. Lu, C. Kim, A. Damascelli, K. M. Shen, D. L. Feng, H. Eisaki, Z. X. Shen, P. K. Mang, et al., Phys. Rev. Lett. **88**, 257001 (2002).
- [23] H. Matsui, K. Terashima, T. Sato, T. Takahashi, S.-C. Wang, H.-B. Yang, H. Ding, T. Uefuji, and K. Yamada, Phys. Rev. Lett. **94**, 047005 (2005).
- [24] C. Kusko, R. S. Markiewicz, M. Lindroos, and A. Bansil, Phys. Rev. B **66**, 140513(R) (2002).
- [25] Q. Yuan, Y. Chen, T. K. Lee, and C. S. Ting, Phys. Rev. B **69**, 214523 (2004).
- [26] K. K. Voo and W. C. Wu, Physica C **417**, 103 (2005).
- [27] H. G. Luo and T. Xiang, Phys. Rev. Lett. **94**, 027001 (2005).
- [28] T. Xiang and J. M. Wheatley, Phys. Rev. Lett. **76**, 134 (1996).
- [29] C. S. Liu, unpublished notes.
- [30] K. Yamada and K. Kurahashi and T. Uefuji and M. Fujita and S. Park and S.-H. Lee and Y. Endoh, Phys. Rev. Lett. **90**, 137004 (2003).